Emergent randomness in the Jaynes–Cummings model

2008 J. Phys. A: Math. Theor. 41 075304

(http://iopscience.iop.org/1751-8121/41/7/075304)

IOP PUBLISHING JOURNAL OF PHYSICS A: MATHEMATICAL AND THEORETICAL

J. Phys. A: Math. Theor. **41** (2008) 075304 (22pp) doi:10.1088/1751-8113/41/7/075304

Emergent randomness in the Jaynes–Cummings model

B M Garraway[1] **and S Stenholm**[2,3]

[1] Department of Physics and Astronomy, University of Sussex, Falmer, Brighton, BN1 9QH, UK
[2] Physics Department, Royal Institute of Technology, KTH, Stockholm, Sweden
[3] Laboratory of Computational Engineering, HUT, Espoo, Finland

Received 9 January 2008
Published 5 February 2008
Online at stacks.iop.org/JPhysA/41/075304

Abstract

We consider the well-known Jaynes–Cummings model and ask if it can display randomness. As a solvable Hamiltonian system, it does not display chaotic behaviour in the ordinary sense. Here, however, we look at the distribution of values taken up during the total time evolution. This evolution is determined by the eigenvalues distributed as the square roots of integers and leads to a seemingly erratic behaviour. That this may display a random Gaussian value distribution is suggested by an exactly provable result by Kac. In order to reach our conclusion we use the Kac model to develop tests for the emergence of a Gaussian. Even if the consequent double limits are difficult to evaluate numerically, we find definite indications that the Jaynes–Cummings case also produces a randomness in its value distributions. Numerical methods do not establish such a result beyond doubt, but our conclusions are definite enough to suggest strongly an unexpected randomness emerging in a dynamic time evolution.

PACS numbers: 42.50.Ct, 42.50.Pq, 03.65.−w

1. Introduction

The Jaynes–Cummings model has become the paradigmatic model for interactions between cavity eigenmodes and atoms. Many features of quantum optics have been elucidated within this model; for a comprehensive review consult [1].

The model is exactly solvable as a quantum system with nontrivial time evolution, which involves dephasing and subsequent recurrences. This behaviour derives from the square-root dependence of the eigenvalues on the integer quantum numbers. It thus constitutes a proof of the photon picture of quantized electromagnetic fields.

Except for the quasiperiodic recurrences, the time evolution seems rather random for initial states significantly different from Fock states. However, we know that an integrable quantum model cannot possibly display chaotic behaviour in the sense used for dynamical

systems. The situation changes, however, if the discrete quantum numbers are replaced by a semi-classically treated average field, see [2]. When the field variable is governed by its own equation of motion, i.e. the Maxwell equations, the ensuing nonlinear system of equations displays chaotic behaviour. This was discussed by Belobrov *et al* [3] and Milonni *et al* [4]. They find that the system is chaotic in the standard sense, but this feature disappears if the rotating wave approximation is applied. The reason is that this introduces an additional conserved quantity, which effectively makes the system of equations two-dimensional; it is known that such a system cannot display chaos. The constant of the motion is destroyed if one adds dissipative terms to the equations, and then the ensuing system is equivalent to the Lorenz system, which is known to be chaotic. This was noticed by Haken already in [5].

In this paper we want to show that the time evolution of expectation values in the Jaynes–Cummings model displays random behaviour in the following sense: take a given value of some expectation of some physical quantity, the population on one of the two levels say. We will ask how often this value occurs. That is, we choose to consider the relative weight of this value during the total time evolution.

Regarded as a random variable, this is interpreted as a probability to observe such a value. We claim that the values of the observable tend to occur randomly with a Gaussian distribution. A related model based on incommensurate oscillation frequencies allows a mathematical proof of this fact. This proof is found in [6], and we call this the Kac model. The square roots of integers encountered in the spectrum of the Jaynes–Cummings model are not entirely of this type, but our numerical work shows that there tends to be enough incommensurability to give the random behaviour for practical purposes.

The phenomenon investigated occurs in the double limit of an infinite number of terms, i.e. infinite number of frequencies, and an infinite time. Such double limits of oscillating functions are difficult to handle numerically. Hence we find it convenient to have the mathematically provable Kac model as a comparison. If we can determine the behaviour of the Jaynes–Cummings model with the same confidence, we regard our conjecture as demonstrated. Full mathematical certainty cannot be achieved numerically.

Finally, we want to point out that the probability distribution obtained cannot as such be interpreted as a probability of values occurring at a fixed time t. The value at time t is always fully determined by the dynamics. The consequence is that the evolution is not ergodic; the distributions of values for all times cannot be assigned as a distribution at a given time. Only if we regard the temporal origin of the evolution to be stochastic can we assign a probability distribution to a given time. Consequently, only if the time origin is unknown, or governed by some random quantity, can the ergodicity of the evolution be restored.

The proof of the mathematical theorem is indicated in section 2; a mathematically more rigorous proof is found in Kac's book [6]. We investigate numerically how the limits utilized in the theorem emerge. In section 2, we also give an analysis for the Jaynes–Cummings model which is suggestive of the result we seek to establish. Then, using the insight gained from the Kac model we apply the result to the Jaynes–Cummings model. Within the numerical limitations of our method, we find the stochastic behaviour established.

2. Formal considerations

2.1. Probability distributions

Let a function $S(t)$ take real values under a variation of the parameter $t \in [-\infty, \infty]$. Then the weight of the set where the function takes on the values between a and b is taken to be the

integral

$$P = P\{b \leqslant S(t) \leqslant a\} \equiv \lim_{T\to\infty} \frac{1}{2T} \int_{-T}^{T} \Theta(b, a; S(t))\, \mathrm{d}t, \tag{1}$$

where the Θ-function is defined by

$$\begin{aligned} \Theta(b, a; x) &= 1 \text{ if } b \leqslant x \leqslant a \\ &= 0 \text{ elsewhere.} \end{aligned} \tag{2}$$

It is easily seen that this function can be represented by the integral

$$\begin{aligned} \Theta(b, a; x) &= \lim_{\varepsilon\to 0} \frac{1}{2\pi \mathrm{i}} \int_{-\infty}^{\infty} \left[\frac{\exp(\mathrm{i}(a-x)\xi) - \exp(\mathrm{i}(b-x)\xi)}{\xi - \mathrm{i}\varepsilon} \right] \mathrm{d}\xi \\ &= \theta(a-x) - \theta(b-x), \end{aligned} \tag{3}$$

where $\theta(x)$ is the ordinary Heaviside function.

We further need to define the Fourier transform of the Θ-function

$$G_{ab}(\eta) = \int_{-\infty}^{\infty} \Theta(b, a; x) \exp(\mathrm{i}x\eta)\, \mathrm{d}x = \frac{\mathrm{e}^{\mathrm{i}a\eta} - \mathrm{e}^{\mathrm{i}b\eta}}{\mathrm{i}\,(\eta - \mathrm{i}\varepsilon)}. \tag{4}$$

These are the tools we need in the derivation below. The formal inverse transform gives

$$\Theta(b, a; x) = \frac{1}{2\pi} \int_{-\infty}^{\infty} G_{ab}(\eta) \exp(-\mathrm{i}x\eta)\, \mathrm{d}\eta. \tag{5}$$

2.2. The Kac model

Define a set of numbers $\{\lambda_1, \lambda_2, \ldots, \lambda_n\}$ such that the linear combination with integer coefficients $\{n_\nu\}$

$$\sum_{\nu=1}^{n} n_\nu \lambda_\nu = 0 \tag{6}$$

implies that $n_\nu = 0$ for $\forall\, \nu$. The numbers are incommensurate. We next form the sums

$$S_n(t) = \sqrt{\left(\frac{2}{n}\right)} \left(\cos\lambda_1 t + \cos\lambda_2 t + \cdots + \cos\lambda_n t\right). \tag{7}$$

The normalization is chosen such that the time average gives

$$\overline{[S_n(t)]^2} = \frac{2}{n} \sum_{\nu,\mu} \overline{\cos\lambda_\nu t \cos\lambda_\mu t} = 1. \tag{8}$$

We now proceed to calculate the probability distribution of the values $S_n(t)$ when the number of terms n goes to infinity. According to (1), the probability for fixed n is given by

$$P_n = P_n\{b \leqslant S_n(t) \leqslant a\} \equiv \lim_{T\to\infty} \frac{1}{2T} \int_{-T}^{T} \Theta(b, a; S_n(t))\, \mathrm{d}t, \tag{9}$$

which we rewrite using the inverse transform of (5)

$$\begin{aligned} P_n &= \frac{1}{2T} \int_{-T}^{T} \frac{1}{2\pi} \int_{-\infty}^{\infty} G_{ab}(\eta) \exp(-\mathrm{i}\eta S_n(t))\, \mathrm{d}\eta\, \mathrm{d}t \\ &= \frac{1}{2\pi} \int_{-\infty}^{\infty} \mathrm{d}\eta\, G_{ab}(\eta) \frac{1}{2T} \int_{-T}^{T} \mathrm{d}t \prod_{\nu=1}^{n} \exp\left[-\mathrm{i}\eta \sqrt{\left(\frac{2}{n}\right)} \cos\lambda_\nu t \right]. \end{aligned} \tag{10}$$

We use for each value of ν the expansion

$$\exp\left[-\mathrm{i}\eta\sqrt{\left(\frac{2}{n}\right)}\cos\lambda_\nu t\right] = \sum_{k_\nu=-\infty}^{\infty} J_{k_\nu}\left(\eta\sqrt{\left(\frac{2}{n}\right)}\right)(-\mathrm{i})^{k_\nu}\ \mathrm{e}^{\mathrm{i}k_\nu\lambda_\nu t}. \tag{11}$$

Inside the product in equation (10), we now find the terms

$$\lim_{T\to\infty}\frac{1}{2T}\int_{-T}^{T}\exp\left[\mathrm{i}\sum_{\nu=1}^{n}k_\nu\lambda_\nu t\right]\mathrm{d}t = \delta\left(\sum_{\nu=1}^{n}k_\nu\lambda_\nu\right). \tag{12}$$

According to our basic assumption (6), the *only* way the delta-function in equation (12) can be non-zero is when the terms with $k_\nu = 0$ are selected. Then the expression (10) becomes

$$\begin{aligned} P_n &= \frac{1}{2\pi}\int_{-\infty}^{\infty}\mathrm{d}\eta\, G_{ab}(\eta)\left[J_0\left(\eta\sqrt{\left(\frac{2}{n}\right)}\right)\right]^n \\ &= \frac{1}{2\pi}\int_{-\infty}^{\infty}\mathrm{d}\eta\, G_{ab}(\eta)\exp\left(-\frac{1}{2}\eta^2\right), \end{aligned} \tag{13}$$

because

$$\lim_{n\to\infty}\left[J_0\left(\eta\sqrt{\left(\frac{2}{n}\right)}\right)\right]^n = \lim_{n\to\infty}\left[1-\left(\frac{\eta^2}{2n}\right)\right]^n = \exp\left(-\frac{1}{2}\eta^2\right). \tag{14}$$

From (13) and (4) we write

$$\begin{aligned} P_\infty &= \frac{1}{2\pi}\int_{-\infty}^{\infty}\mathrm{d}\eta\int_{-\infty}^{\infty}\mathrm{d}x\,\Theta(b,a;x)\exp(\mathrm{i}x\eta)\exp\left(-\frac{1}{2}\eta^2\right) \\ &= \frac{1}{\sqrt{2\pi}}\int_{-\infty}^{\infty}\Theta(b,a;x)\exp\left(-\frac{1}{2}x^2\right)\mathrm{d}x, \end{aligned} \tag{15}$$

because

$$\int_{-\infty}^{\infty}\mathrm{d}\eta\exp(\mathrm{i}x\eta)\exp\left(-\frac{1}{2}\eta^2\right) = \sqrt{2\pi}\exp\left(-\frac{1}{2}x^2\right). \tag{16}$$

Using (3) we can write (15) as

$$P_\infty = P\{b\leqslant S_\infty(t)\leqslant a\} = \frac{1}{\sqrt{2\pi}}\int_b^a\exp\left(-\frac{1}{2}x^2\right)\mathrm{d}x. \tag{17}$$

This proves that, in the limit of an infinite number of terms, the values of the function $S_n(t)$ have a Gaussian distribution with width equal to unity. The value of the width follows, of course, from our normalization (8), but the essential assumption is the linear independence (6) of our parameters $\{\lambda_\nu\}$.

2.3. The Jaynes–Cummings model

The Jaynes–Cummings model [1] is defined by the Hamiltonian

$$H = H_1 + H_2, \tag{18}$$

where

$$\begin{aligned} H_1 &= \hbar\Omega\left(b^\dagger b + \frac{1}{2}\sigma_3\right) \\ H_2 &= \frac{\hbar}{2}\Delta\Omega\sigma_3 + \hbar g(\sigma^+ b + \sigma^- b^\dagger); \end{aligned} \tag{19}$$

here the operators $\{b, b^\dagger\}$ obey Boson commutation relations and $\{\sigma^+, \sigma^-, \sigma_3\}$ are Pauli operators. The detuning is defined as

$$\Delta\Omega = \omega - \Omega, \tag{20}$$

where $\hbar\omega$ is the level separation in the two-level system and Ω is the frequency of the Boson field.

In presenting the exact solution, we set $\Delta\Omega = 0$, which is expedient for our purpose. The solution may be written as

$$\begin{aligned}|\Psi(t)\rangle = \sum_{n=0}^{\infty} a_n^0 \big[& c_0^+(\cos\varphi_{n+1}|+, n\rangle - \mathrm{i}\sin\varphi_{n+1}|-, n+1\rangle) \\ & + c_0^-(\cos\varphi_n|-, n\rangle - \mathrm{i}\sin\varphi_n|+, n-1\rangle)\big].\end{aligned} \tag{21}$$

Here we have defined

$$\varphi_n \equiv \sqrt{n} g t \tag{22}$$

and in (21) we let $|\pm\rangle$ and $|n\rangle$ be the eigenstates of σ_3 and $b^\dagger b$. The coefficients $\{a_n^0\}$ determine the initial distribution of the photons and the coefficients $\{c_0^-, c_0^+\}$ the initial value of the two-level system. We next project on the two levels of the atomic system

$$\begin{aligned}\langle +|\Psi(t)\rangle &= \sum_{n=0}^{\infty} a_n^0\big(c_0^+\cos\varphi_{n+1}|n\rangle - \mathrm{i}c_0^-\sin\varphi_n|n-1\rangle\big) \\ \langle -|\Psi(t)\rangle &= \sum_{n=0}^{\infty} a_n^0\big(-\mathrm{i}c_0^+\sin\varphi_{n+1}|n+1\rangle + c_0^-\cos\varphi_n|n\rangle\big).\end{aligned} \tag{23}$$

We consider two cases

$$\begin{aligned}&(a) \quad c_0^- = 1, c_0^+ = 0; \\ &(b) \quad c_0^- = 0, c_0^+ = 1.\end{aligned} \tag{24}$$

The corresponding probabilities of occupation on the levels are given by

$$\begin{aligned}P_+^a &= |\langle +|\Psi_a\rangle|^2 = \sum_{n=0}^{\infty}\left|a_{n+1}^0\right|^2\sin^2\varphi_{n+1} = \sum_{n=0}^{\infty}\left|a_n^0\right|^2\sin^2\varphi_n \\ P_-^a &= |\langle -|\Psi_a\rangle|^2 = \sum_{n=0}^{\infty}\left|a_n^0\right|^2\cos^2\varphi_n \\ P_+^b &= |\langle +|\Psi_b\rangle|^2 = \sum_{n=0}^{\infty}\left|a_n^0\right|^2\cos^2\varphi_{n+1} \\ P_-^b &= |\langle -|\Psi_b\rangle|^2 = \sum_{n=1}^{\infty}\left|a_{n-1}^0\right|^2\sin^2\varphi_n = \sum_{n=0}^{\infty}\left|a_n^0\right|^2\sin^2\varphi_{n+1}.\end{aligned} \tag{25}$$

The summation variables can be shifted because $\varphi_0 = 0$.

Using the trigonometric identities

$$\begin{aligned}\sin^2\varphi &= \tfrac{1}{2}(1 - \cos 2\varphi) \\ \cos^2\varphi &= \tfrac{1}{2}(1 + \cos 2\varphi)\end{aligned} \tag{26}$$

we obtain the results

$$P_{\pm}^{a} = \tfrac{1}{2}(1 \mp S^{(0)}) \qquad P_{\pm}^{b} = \tfrac{1}{2}(1 \pm S^{(1)}). \tag{27}$$

The sums are given by

$$S^{(k)} = \sum_{n=0}^{\infty} \left|a_n^0\right|^2 \cos 2\varphi_{n+k} \qquad (k = 0, 1). \tag{28}$$

If we choose the case (a) we may deal with the infinite sum

$$S = S^{(0)}/N = \frac{\sqrt{2}}{N} \sum_{n=0}^{\infty} c_n \cos 2gt\sqrt{n}, \tag{29}$$

where we choose

$$c_n = \frac{\left|a_n^0\right|^2}{\sqrt{2}} \tag{30}$$

along with a normalization N which will be determined later. In terms of dimensionless time $2gt$, this is very similar to the sum (7) with $\lambda_\nu = \sqrt{\nu}$. These do not form a sequence of incommensurate numbers, but we want to investigate the applicability of the result in section 2.2 to this case. An additional difference is the normalization of the coefficients in the present case. Instead of (8) the quantum-mechanical normalization of a state vector requires

$$\sum_{n=0}^{\infty} \left|a_n^0\right|^2 = 1, \tag{31}$$

which, because of the connection (30), requires in equation (29) the presence of the normalization N, i.e. it forces us to rescale the ensuing distribution, vide infra.

We also want to put in an initial photon distribution; one such is given by the coherent state which we will use in the numerical calculations. It is smooth and extends over several states; we expect this to be enough to give the random distribution, if such a distribution is to emerge. We have not carried out a systematic investigation of the dependence of the result on the initial distribution. The coherent state suffices to establish the existence of the random distribution even in the case of a sum over square roots instead of one over incommensurate frequencies only.

2.4. Randomness in the Jaynes–Cummings case

The derivation of the Gaussian distribution in section 2.2 follows from the exact incommensurability relation (6) and the exact mathematical limit (14). In the Jaynes–Cummings case neither one can be taken as fully satisfied. It is, however, possible to obtain the same result utilizing a less rigorous but physically justifiable argument.

Instead of the sum (7) we will deal with the normalized sum (29) with its different limits (0 to ∞, rather than 1 to n). In a way similar to the derivation of equation (10) from equation (7), we can obtain a new version of equation (10), but this time the second integral reads

$$\frac{1}{2T} \int_{-T}^{T} \mathrm{d}t \prod_{k=0}^{\infty} \exp\left[-\mathrm{i}\frac{\eta\sqrt{2}c_k}{N} \cos \lambda_k t\right] \equiv E_t \left[\prod_{k=0}^{\infty} K_k\right], \tag{32}$$

where E_t denotes a time average and the K_k represent the exponential terms in the product. Assuming the frequencies λ_k to be 'sufficiently' different, we surmise that we may take the average over the individual terms in the product separately. Then for each one of the terms we

obtain

$$E_t[K_k] = E_t\left[\exp\left(-\mathrm{i}\frac{\eta\sqrt{2}c_k}{N}\cos\lambda_k t\right)\right]$$
$$= \sum_{\nu=0}^{\infty}\frac{(-\mathrm{i}\eta\sqrt{2}c_k/N)^{2\nu}}{2\nu!}E_t[\cos^{2\nu}\lambda_k t], \tag{33}$$

because the odd terms average to zero. Because of the relation [7],

$$\frac{2}{\pi}\int_0^{\pi/2}\cos^{2\nu}x\,\mathrm{d}x = \frac{(2\nu)!}{2^{2\nu}(\nu!)^2}, \tag{34}$$

equation (33) becomes

$$E_t[K_k] = \sum_{\nu=0}^{\infty}\frac{\left(-\eta^2c_k^2/2N^2\right)^{\nu}}{(\nu!)^2} = J_0\left(\frac{\sqrt{2}\eta c_k}{N}\right)$$
$$\approx\left(1-\frac{\eta^2c_k^2}{2N^2}\right)\approx\exp\left(-\frac{\eta^2c_k^2}{2N^2}\right). \tag{35}$$

We now introduce the normalization condition

$$\frac{1}{N^2}\sum_{k=0}^{\infty}c_k^2 = 1, \tag{36}$$

which is consistent with equation (8) in the case $c_k = 1/\sqrt{k}$, $N = 1$, $1 \leqslant k \leqslant n$, as $n \to \infty$. Then equation (32) gives

$$E_t\left[\prod_{k=0}^{\infty}K_k\right] = \exp\left(-\frac{\eta^2}{2}\right). \tag{37}$$

As before, the Fourier transform of this gives the normalized probability distribution

$$p(x) = \frac{1}{\sqrt{2\pi}}\exp\left(-\frac{1}{2}x^2\right). \tag{38}$$

The derivation above replaces the condition of absolute incommensurability by the more physically motivated assumption of separate time averages. In the end the results are equivalent. Also the approximation in (35) may be justified by the normalization (36); if enough of the many terms differ from zero, and the distribution is reasonably smooth, each term in the sum must become very small and hence justify the approximation. These arguments cannot, however, replace the exactness of the Kac model, but suggest that its conclusions may hold under less stringent requirements. This is what we want to establish in the case of the Jaynes–Cummings model.

3. Numerical checks

3.1. General considerations and initial state

We consider the asymptotic behaviour of sums of the type

$$S_n(t) = \frac{\sqrt{2}}{N}\sum_{k=0}^{n}c_k\cos\lambda_k t, \tag{39}$$

when $n \to \infty$ and we average the distribution of the values of S_n over an infinite time $t \to \infty$. The behaviour of this double limit is nontrivial to establish numerically, but the behaviour can be suggested by certain criteria to be presented below.

In the Kac model, we have the simple relations

$$\begin{aligned} c_k &= \frac{1}{\sqrt{n}}, \qquad \text{for} \quad 1 \leqslant k \leqslant n, \\ \lambda_k &= \{\text{incommensurate numbers}\}. \end{aligned} \tag{40}$$

The normalization is

$$\sum_{k=1}^{n} c_k^2 = 1 \tag{41}$$

so that $N = 1$ in equation (39). The mathematical demonstration for the Kac model in section 2.2 shows that the resulting distribution should be the Gaussian

$$p(x) = \frac{1}{\sqrt{2\pi}} \exp\left(-\frac{x^2}{2}\right). \tag{42}$$

That is, the distribution p of the values of S_n obeys

$$\lim_{n\to\infty} p(S_n) = \lim_{n\to\infty} \frac{1}{\sqrt{2\pi}} \exp\left(-\frac{S_n^2}{2}\right) \to \frac{1}{\sqrt{2\pi}} \exp\left(-\frac{S^2}{2}\right), \tag{43}$$

where $S = S^{(0)}/N$ as in equation (29). Because this result is shown to be exact, it presents a test case: if this can be established with a certain numerical confidence, the same confidence should be indicative of the behaviour of other cases.

Our interest is the Jaynes–Cummings model, where $\lambda_k \propto \sqrt{k}$, as may be seen by comparing the two series (39) and (29). Here, however, the normalization is different and the sum has an infinite number of terms. The condition arrived at in section 2.4, equation (36), together with equation (30), $c_k = |a_k^0|^2/\sqrt{2}$, implies the condition

$$\frac{1}{2N^2} \sum_{k=0}^{\infty} \left|a_k^0\right|^4 = 1. \tag{44}$$

It is now clear that, in the Jaynes–Cummings model case, the normalization factor $N \neq 1$ and it depends on the initial state because of the original quantum-mechanical normalization (31), $\sum_{k=0}^{\infty} \left|a_k^0\right|^2 = 1$. Indeed, this normalization, taken together with equation (44), implies that $N < 1/\sqrt{2}$, since we must have $\sum_{k=0}^{\infty} \left|a_k^0\right|^4 \leqslant 1$. This means that, without rescaling the sum S by the factor N in equation (29), the width of the distribution of the Jaynes–Cummings sum $S^{(0)}$ would be rather less than unity.

For an initial quantum state we are going to use the coherent state as a reference in our model. That is, we let

$$\left|a_k^0\right|^2 = \mathrm{e}^{-\bar{n}} \frac{\bar{n}^k}{k!}, \tag{45}$$

so that from equation (44) we find

$$N = \exp(-\bar{n})\sqrt{I_0(2\bar{n})/2} \approx \frac{1}{2(\pi\bar{n})^{1/4}}, \tag{46}$$

where I_0 is a modified Bessel function. The approximation in equation (46) holds for large photon number, $\bar{n} \gg 1$. The approximate result can also be easily found from

$$\mathrm{e}^{-\bar{n}} \frac{\bar{n}^k}{k!} \approx \frac{1}{\sqrt{2\pi\bar{n}}} \exp\left[-\frac{(k-\bar{n})^2}{2\bar{n}}\right], \tag{47}$$

so that

$$N^2 = \frac{1}{2} \sum_{k=0}^{\infty} \left|a_k^0\right|^4 \approx \frac{1}{4\pi\bar{n}} \int_{-\infty}^{\infty} \exp\left[-\frac{(k-\bar{n})^2}{\bar{n}}\right] \mathrm{d}k = \frac{1}{4\sqrt{\pi\bar{n}}}. \tag{48}$$

For a coherent state with a given $\bar{n}$, this factor N scales the Gaussian distribution for S to one expected to have unit width. (See equation (29).)

A restriction on the Jaynes–Cummings model as compared with the Kac model is that since the probabilities (27) must be less than unity, the scaled sum (39) is limited to the intervals

$$|S(t)| \leqslant \frac{1}{2N}, \tag{49}$$

as $n \to \infty$. For the coherent state this means that $S(t)$ is bounded by $(\pi\bar{n})^{1/4}$ for large $\bar{n}$. Whilst $\bar{n}$ is finite this will prevent the emergence of a Gaussian to exact precision. The resulting considerations will be taken into account when the evidence for randomness is evaluated below.

3.2. Numerical tests

3.2.1. Methods. The numerical tests look at the two models (Kac and Jaynes–Cummings) and in each case the sum $S_n(t)$, equation (39), is evaluated for a large number of sampling times. For the Kac model c_k and λ_k are given in equation (40). For the incommensurate numbers in the cosine we use the square roots of consecutive prime numbers starting at 2. For the Jaynes–Cummings model c_k is given by equation (30) and we have $\lambda_k = \sqrt{k}$ where the k are integers starting at zero. This implies a scaled dimensionless time in the Jaynes–Cummings model case: $2gt \longrightarrow t$.

The limit n of the sum (39) is necessarily finite: in the Kac case this is consistent with the model, in the Jaynes–Cummings model we choose a limit n rather larger than $\bar{n}$ (actually $2.5 \times \bar{n}$) to capture the significant contributions to the sum.

The time sampling is regular and is chosen at an incommensurate frequency a little higher than the highest cosine frequency present in the sum S_n, i.e. for the sampling time interval we have

$$\Delta t = 1/\lambda_n. \tag{50}$$

For the Kac model, for example, the results presented in section 3.2.2 involve values of n no higher than 200, so if the final sampling time is $t_f = 2 \times 10^6$ we have included up to 70 million sample times (which start at $t = 0$). We have checked if there is any difference between the regular sampling and sampling at random times (up to a limit t_f). With random sampling the trends, in general, remain the same, though the differences from Gaussian can be larger.

Since the normal distribution (38) has a unit width, one of the statistical tests of the results is simply to compute the standard deviation σ of the time sampled values of S_n; the results in the figures (in sections 3.2.2 and 3.2.3) show $\sigma - 1$ so that deviations from the expected unit width are more easily seen.

In order to go beyond simple statistical quantities, we use as a measure of the difference between the normal distribution (38) and the distribution of sampled values of S_n, the Kolmogorov–Smirnov distance D as given by the algorithm in [8]. The Kolmogorov–Smirnov distance D is the maximum distance between the *cumulative* distributions. For the ideal distribution (38) the cumulative distribution is simply given by an error function. The maximum deviation of the sampled data from this error function is given by D and provides a useful measure of differences over the whole distribution function.

It is also useful to visualize the probability distributions by binning the values of $S_n(t)$ at the sampled time points. Typically we use $N_{\text{bin}} = 600$ bins at values x_j spread between ± 4. The result is normalized to unit probability. The resulting numerical distribution $p_{\text{bin}}(x_j)$ is expected to be an approximation to the ideal distribution $p(x)$, as given in equation (38). The difference between these distributions, $p_{\text{bin}}(x_j) - p(x_j)$, is expected to have a scatter,

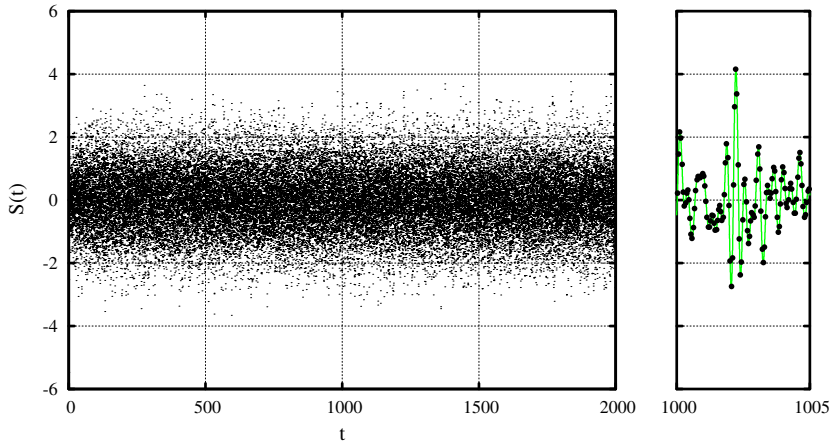

Figure 1. (Left frame) For the Kac model case we show typical time sampled points up to a rather low scaled time $t \to 2000$ to show the features of the time evolution. The number of terms in the Kac sum S is $n = 100$. In the later analysis and figures the sum S is sampled to much later times, up to $t_f = 2.0 \times 10^6$. (Right frame) Shows a narrow window of data from the left frame, with dots indicating sampled time points and the line indicating the continuous value of the sum $S(t)$.

and to measure this it is useful to define a simple RMS deviation for the absolute values $p_{\text{bin}}(x_j) - p(x_j)$. Thus we define the quantity ΔP through

$$\Delta P^2 = \frac{1}{N_{\text{bin}}} \sum_{j=1,N_{\text{bin}}} [p(x_j) - p_{\text{bin}}(x_j)]^2. \tag{51}$$

Given that most of the 'noise' in $p_{\text{bin}}(x_j) - p(x_j)$ is located around the origin it should be noted that ΔP is sensitive to the bin limits, so these are kept constant throughout.

3.2.2. Kac model. An example of the time series S for the Kac model is given in figure 1 for the case $n = 100$. On the long time-scale (left part of figure 1) the data look essentially chaotic. The largest value of S is at $t = 0$ when the terms all add to a value of $\sqrt{2 \times 100}$ (an extreme point excluded by the y-range selected in the figure). On a short time-scale, such as in the narrow region selected on the right of figure 1, it is possible to see a correlation between successive time points.

In the case of the Kac model, we know from the mathematical proof that the Gaussian limit for the distribution should emerge accurately. Thus the confidence acquired here may serve as a test of the power of our numerical method and the reliability of our conclusions.

The claim we investigate is that the emerging distribution is the normalized Gaussian. In figure 2 both these distributions $p_{\text{bin}}(x)$ and $p(x)$ are shown and the fit appears to be very good. To investigate further, we display the difference in figure 3. When the number of terms included grows from $n = 52$ to $n = 200$, we observe a tendency to shrink the difference. At best the difference is of the order 10^{-3}, which we consider to be satisfactory.

We have to consider carefully the double limit, $n \to \infty$ and $t \to \infty$. The first thing to establish is the convergence. To this end we consider the question of whether the raw data tend to approach the unit width expected; this is the σ-test. In figure 4, the deviation from unity is shown as function of the averaging time t_f. The result is displayed for three different cut-off values in the sums. The increase of terms decreases the scatter of the points, and for

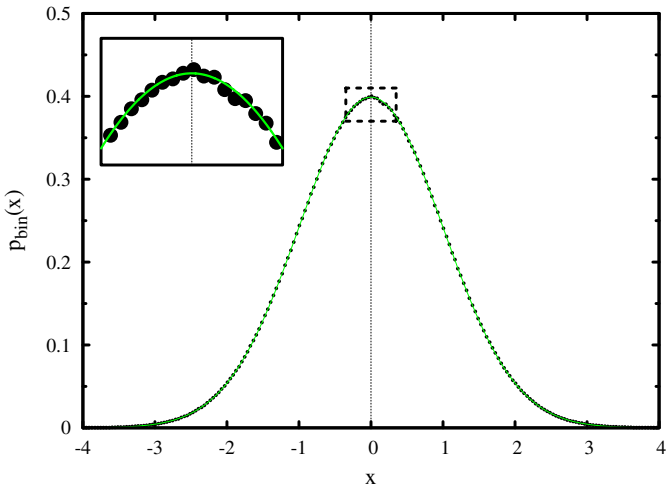

Figure 2. The binned distribution $p_{\text{bin}}(x)$ for the Kac model (dots) and the reference normal distribution (38) (shown as a line). In the binned case: $t_f = 2.0 \times 10^6$ and the number of terms in the series (7) is $n = 200$ (dots). Only 200 of the 600 bin values are shown in the figure. The region marked with a rectangle is shown on an expanded scale in the inset.

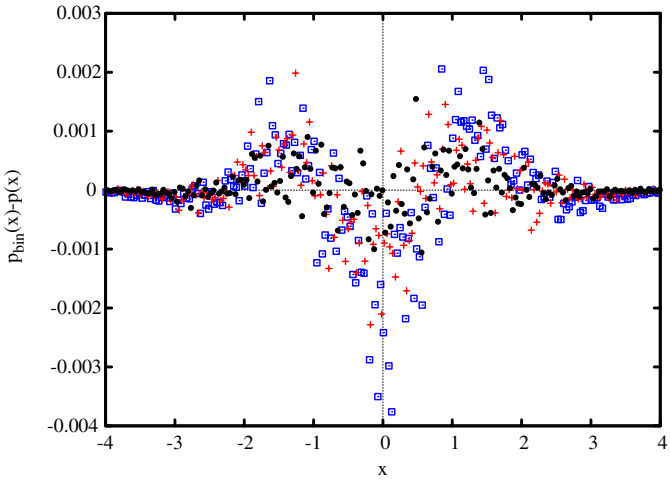

Figure 3. Difference between the binned distribution of the Kac model and the normal distribution (38). The sampling is taken to a final time $t_f = 2.0 \times 10^6$. The number of terms in the sum (7) is: $n = 52$ (squares), $n = 100$ (crosses), $n = 200$ (circles). The circles appear to show noise, but this arises from the finite, though large, sampling rather than from numerical error. Only every third bin is shown.

the largest number ($= 200$) a steady decrease is convincingly emerging. For the longest time used ($t = 2 \times 10^6$) a value near 10^{-6} has been reached. We are convinced that longer times would cause this to drop steadily towards zero.

In order to test the validity of the distribution assumed, we bin the numerical data (see above) and test how well they are represented by the Gaussian. The test is the RMS value.

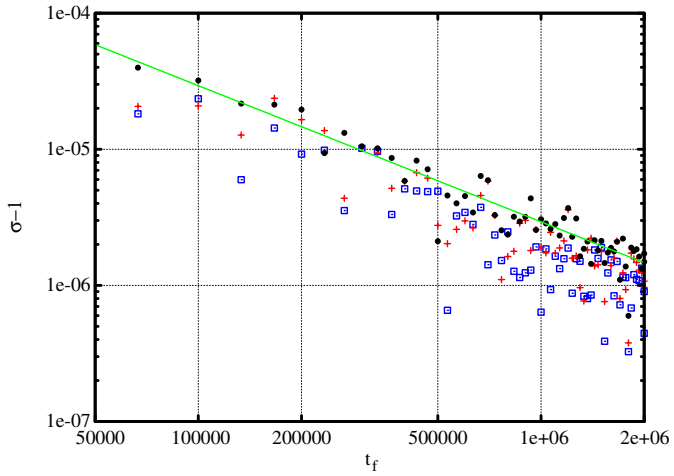

Figure 4. For the Kac model we show the statistical width σ (plotted as $\sigma - 1$ on a log scale) as a function of the final time t_f (up to $t_f = 2.0 \times 10^6$). The number of terms in the sum (7) is: $n = 52$ (squares), $n = 100$ (crosses), $n = 200$ (circles). The straight line shows a simple fit to the circles ($\simeq 3.0/t_f$) to guide the eye.

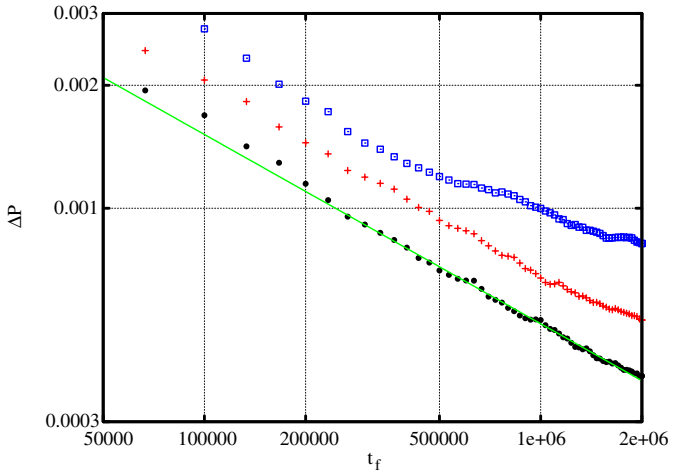

Figure 5. For the Kac model we show on a log–log scale the RMS deviation ΔP between the binned and model distributions, equation (51), over the bin range and as a function of the final time t_f (up to $t_f = 2.0 \times 10^6$). The number of terms in the sum (7) is: $n = 52$ (squares), $n = 100$ (crosses), $n = 200$ (circles). The straight line shows a power-law fit to the circles to guide the eye.

In figure 5 we see how this is improved with averaging time. For increased number of terms the convergence is rapidly improved. Figure 6 shows the dependence of the RMS value ΔP on the number of terms included. Here we can also clearly see the strong improvement with increasing averaging time. For the final values, $t = 2 \times 10^6$ and $n = 200$, we find a value $<4 \times 10^{-4}$.

A standard test of the validity of a given distribution to describe a set of data is the Kolmogorov–Smirnov (K–S) value D. The K–S distance is shown for the Gaussian compared to the Kac model as function of time in figure 7. The figure shows that for a given n a non-zero limiting value is established for a sufficient number of time samples, i.e. for large enough t_f.

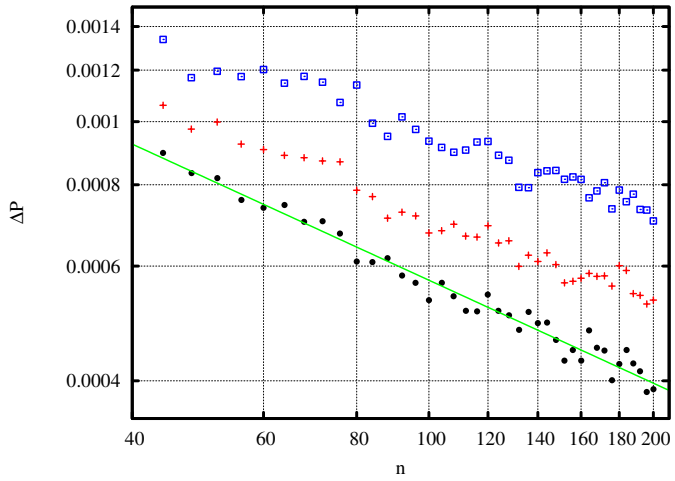

Figure 6. The RMS deviation ΔP, equation (51), between the binned (Kac) and model distributions over the bin range and as a function of the number of terms n in the sum (7) (from 44 to 200). The final time is: $t_f = 0.5 \times 10^6$ (squares), $t_f = 1.0 \times 10^6$ (crosses), $t_f = 2.0 \times 10^6$ (circles). The plot is on a log scale and the straight line shows a power-law fit to the circles to guide the eye.

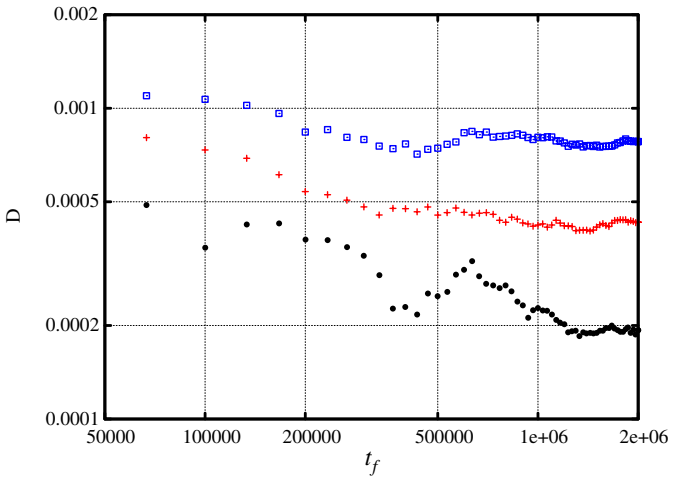

Figure 7. For the Kac model data and the model distribution (38) we show the Kolmogorov–Smirnov distance D between the respective cumulative distributions. This is seen on a log–log scale and as a function of the final time t_f (up to $t_f = 2.0 \times 10^6$). The number of terms in the sum (7) is: $n = 52$ (squares), $n = 100$ (crosses), $n = 200$ (circles).

This suggests strongly that for finite n there is a difference between the two distributions. The finite limiting value, as a function of t_f, can be understood because once there are enough data to establish the small difference between the distributions, additional sampling will not change the K–S result significantly. In addition, we note that the limiting value reduces as the number of terms n increases. This is seen for the three sets of data in figure 7, and also in figure 8, which gives the dependence on n for several large values of t_f. These results support the contention that the asymptotic behaviour has been reached. The confidence limit reached is of the order 2×10^{-4}.

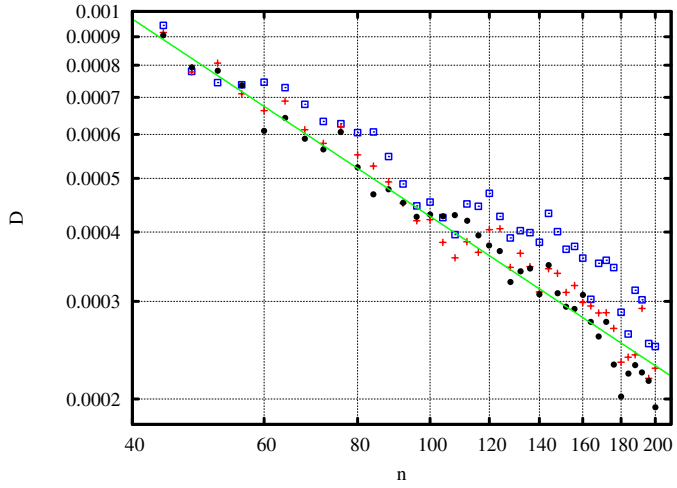

Figure 8. For the Kac model we see on a log–log scale the Kolmogorov–Smirnov distance D between the cumulative distributions as a function of the number of terms n in the sum (7) (from 44 to 200). The final time is: $t_f = 0.5 \times 10^6$ (squares), $t_f = 1.0 \times 10^6$ (crosses), $t_f = 2.0 \times 10^6$ (circles). The straight line shows a power-law fit to the circles to guide the eye.

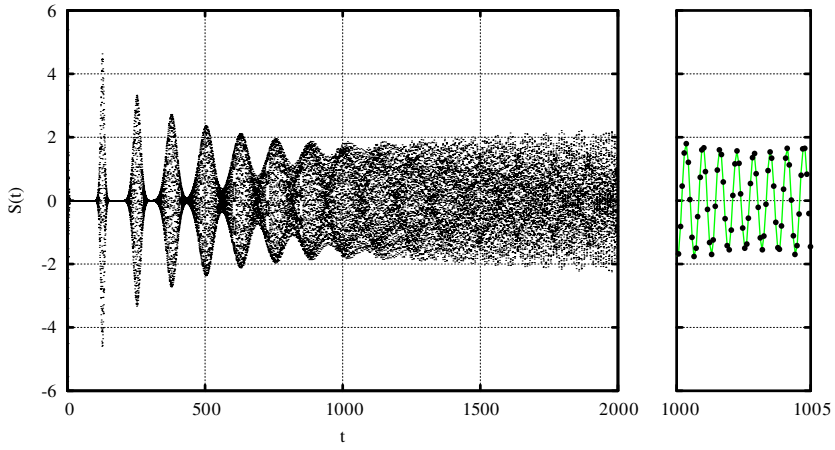

Figure 9. For the Jaynes–Cummings model case we show typical time sampled points of the sum S as in figure 1. The coherent state is chosen with $\bar{n} = 100$. As in figure 1 the right frame shows a narrow window taken from the left frame with dots indicating sampled time points and the line indicating the continuous value of the sum $S(t)$ in the Jaynes–Cummings case.

The numerical investigations of the Kac model suggest that our approach can verify the Gaussian conclusion to an accuracy of order 10^{-4}. For the rest of this investigation, we assume this to be a satisfactory level of confidence in our result.

3.2.3. The Jaynes–Cummings model. An example of the time series $S(t)$ is seen in figure 9 for the Jaynes–Cummings model case with an initial coherent state with an average of 100 photons. On a long time-scale (left part of figure) the time sampled points demonstrate the collapse and revival features first reported in [9]. The revivals appear periodically, but

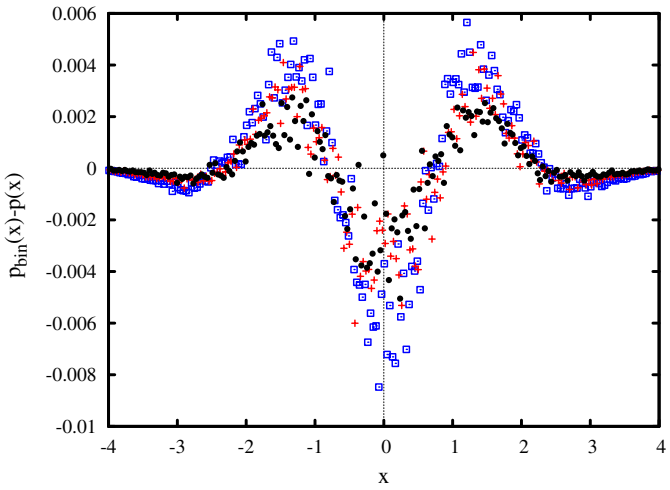

Figure 10. For the Jaynes–Cummings model case we show the difference between the binned distribution and the normal distribution (38) as in figure 3 for the Kac model. The final sample time is $t_f = 2.0 \times 10^6$. The mean number of photons is: $\bar{n} = 25$ (squares), $\bar{n} = 50$ (crosses), $\bar{n} = 100$ (circles). Only every third bin is shown.

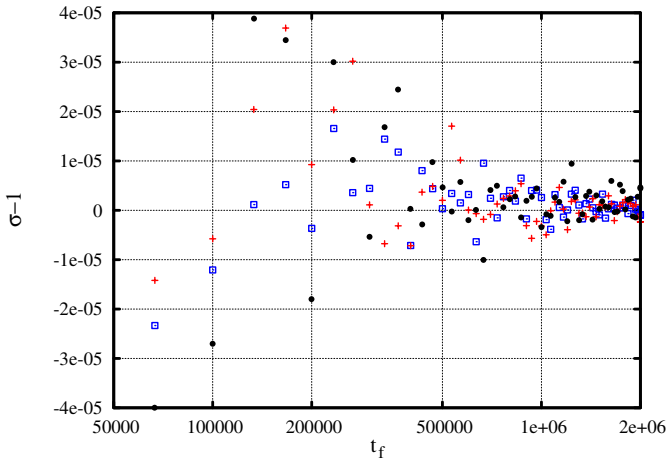

Figure 11. The statistical width σ (shown as $\sigma - 1$) for the Jaynes–Cummings model case. The final sample time t_f is shown on a log scale (up to $t_f = 2.0 \times 10^6$). The initial coherent state has a mean number of photons $\bar{n} = 25$ (squares), $\bar{n} = 50$ (crosses) and $\bar{n} = 100$ (circles).

they broaden and eventually they merge and a more chaotic looking region appears which is reminiscent of the Kac model case seen in figure 1. However, as in the Kac model, there are correlations on a short time-scale, as can be seen in the right part of figure 9.

Next we need to investigate the conjecture that even in the Jaynes–Cummings case the time averaged occurrence of a value is asymptotically producing a Gaussian distribution. In this case the time evolution is determined by a Hamiltonian, and there are essentially two questions: do we find a Gaussian distribution, and is this really the genuine asymptotic distribution? We will suggest answers to both queries by utilizing the methods applied to the Kac model.

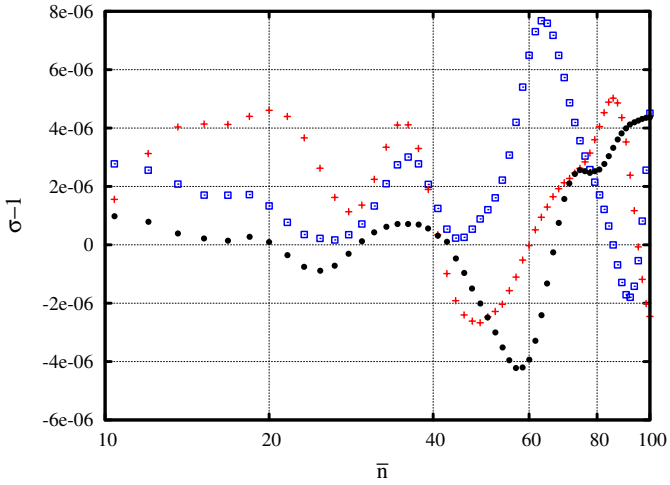

Figure 12. For the Jaynes–Cummings model we show the statistical width σ (shown as $\sigma - 1$) as a function of the mean photon number $\bar{n}$ (from 10 to 100 on a log scale). The final sample time is: $t_f = 0.5 \times 10^6$ (squares), $t_f = 1.0 \times 10^6$ (crosses), $t_f = 2.0 \times 10^6$ (circles).

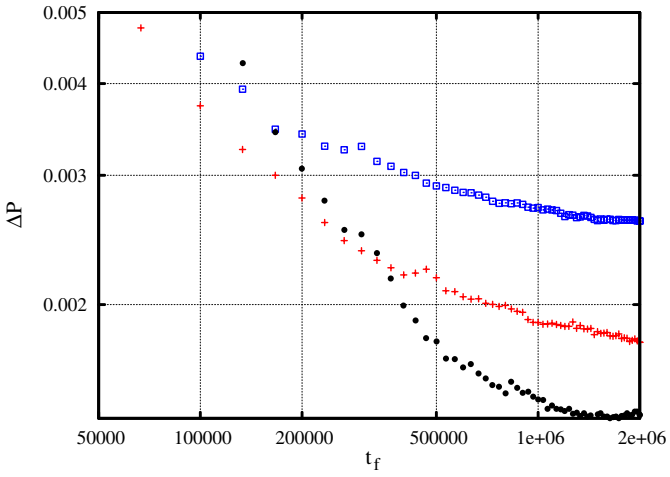

Figure 13. For the Jaynes–Cummings model case we show the RMS deviation ΔP between the binned and model distributions over the bin range. The final time t_f is seen on a log scale (up to $t_f = 2.0 \times 10^6$). The average photon number of the initial coherent state is $\bar{n} = 25$ (squares), $\bar{n} = 50$ (crosses), $\bar{n} = 100$ (circles).

The fit to the Gaussian is tested in figure 10. The deviations are of the same order as for the Kac model in figure 3. The spread σ, as a function of time, is shown in figure 11. The improvement with the increased number of terms is clear and settles down as the number of time samples increases with final time t_f. For the longest time used, 2×10^6, the dispersion differs by much less than 10^{-5}. The spread σ is seen as a function of $\bar{n}$ in figure 12 for selected times t_f. At each of these times this figure does not seem to indicate any convergence with increasing $\bar{n}$. This derives from the fact that because of the deterministic time evolution,

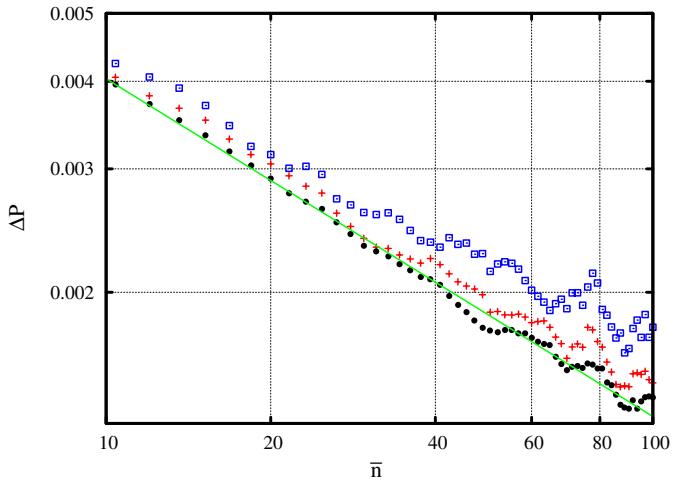

Figure 14. For the Jaynes–Cummings model case we show the RMS deviation ΔP between the binned and model distributions over the bin range and as a function of the mean photon number $\bar{n}$ (from 10 to 100 on a log–log scale). The final sample time is: $t_f = 0.5 \times 10^6$ (squares), $t_f = 1.0 \times 10^6$ (crosses), $t_f = 2.0 \times 10^6$ (circles). The straight line shows a power-law fit to the circles to guide the eye.

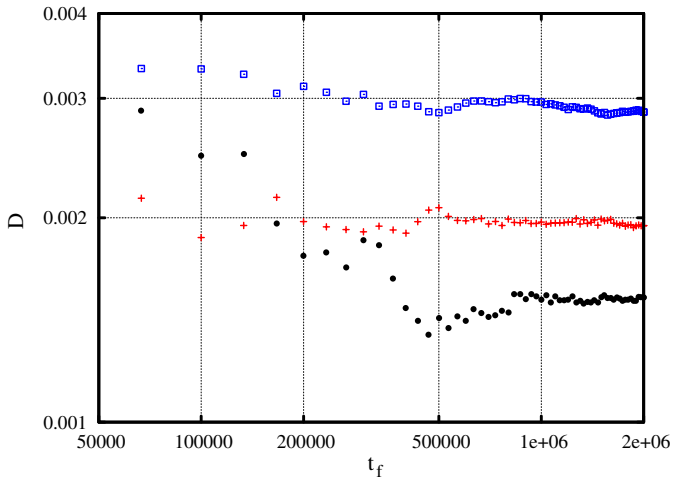

Figure 15. For the Jaynes–Cummings model case we show on a log–log scale the Kolmogorov–Smirnov distance D between the cumulative distributions as a function of the final time t_f (up to $t_f = 2.0 \times 10^6$). The mean photon number is $\bar{n} = 25$ (squares), $\bar{n} = 50$ (crosses), $\bar{n} = 100$ (circles).

the value of $\sigma - 1$ depends strongly on the final time t_f in the evaluation of the averages. Staying at the level 10^{-6}, the result fluctuates deterministically. This is discussed further in the appendix. Binning the numerical data and comparing to the Gaussian, we find the RMS averages in figure 13, where the convergence with the number of terms is clearly seen. The dependence on $\bar{n}$ is shown in figure 14. The values at large $\bar{n}$ indicate an agreement to order $\sim 10^{-3}$, which is one order of magnitude worse than in the Kac model. However, the averaged

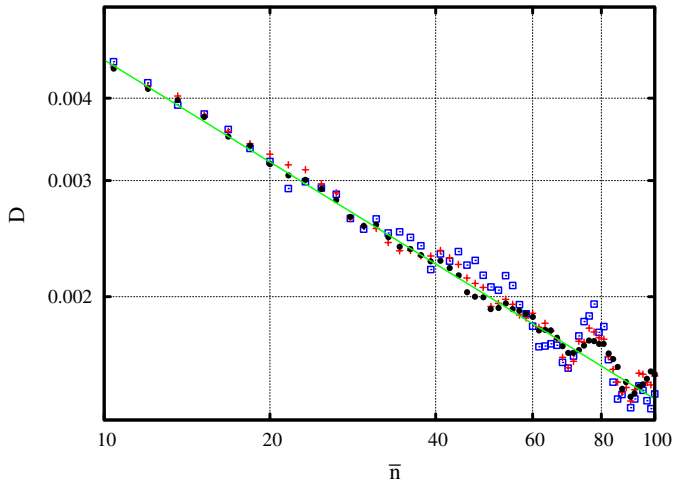

Figure 16. For the Jaynes–Cummings model case we show on a log–log scale the Kolmogorov–Smirnov distance D between the cumulative distributions as a function of the mean photon number $\bar{n}$ (from 10 to 100). The final sample time is: $t_f = 0.5 \times 10^6$ (squares), $t_f = 1.0 \times 10^6$ (crosses), $t_f = 2.0 \times 10^6$ (circles). The straight line shows a power-law fit to the circles.

deviations in figures 13 and 14 demonstrate the convergence in a more convincing manner than in figure 12.

The validity of the Gaussian distribution is again tested by the K–S distance. The result as a function of averaging time is shown in figure 15 and shows convergence to a finite value for the final time selected, as seen in the Kac model (figure 7). The improvement with increasing $\bar{n}$ is displayed in figure 16. Again an accuracy of order 10^{-3} is found as $\bar{n} \to 100$.

4. Conclusions

We have found that our numerical methods verify the Gaussian proposition to within an accuracy of the order 10^{-4} in the case of the Kac model. Both the convergence of the raw data and the numerical binning support this conclusion. We also conclude that convergence with respect to increasing averaging time is reached in the calculations.

For the Jaynes–Cummings model, the calculations suggest that the data are convincingly described by a Gaussian distribution. Considering both the time convergence, figures 11 and 13, and the convergence with increasing $\bar{n}$, figures 12 and 14, we see that the limit has been reached. As $\bar{n}$ increases we note that in effect the number of contributory terms to the sum (39) increases. The confidence of the Gaussian assignment for the Kac model is measured by the K–S distance. This is of order 10^{-4}, as seen in figures 7 and 8. For the Jaynes–Cummings model the corresponding number is one order of magnitude worse, 10^{-3} in figures 15 and 16. The question arises, whether this is a numerical accident or mirrors a deviation from the Gaussian proposed.

The fact that there is a limiting distribution is strongly suggested by the data and the tests. However, this distribution may be only approximately a Gaussian. That this is the case may be suggested from two of the properties of the Jaynes–Cummings model. Firstly, as mentioned in section 3.1, the expectation value of a Pauli spin variable is restricted to the interval $[-1, 1]$. This prevents the wings of the distribution from being accurately described. An effect expected is that, for finite $\bar{n}$, there may occur more probability

in the wings than the Gaussian suggests. However, as $\bar{n}$ increases, the normalization N reduces (see equation (46)) and therefore the bound of $1/(2N)$ on the scaled sum S increases (equation (49)). As a result it is possible for the probability distribution to match increasingly closely a Gaussian as $\bar{n}$ increases.

A second property is obtainable from the known time evolution of the model. The recurrences have envelopes which tend to accumulate occurrences near their turning points. This tends to add weight at each flank of the distribution with an accompanying depletion of weight at the peak of the distribution.

We get some support for the existence of a difference by comparing the accuracy of the Jaynes–Cummings fit in figure 10 to the corresponding one for the Kac model in figure 3. In the latter case, the deviation appears to represent a good deal of numerical noise. Increasing the number of terms shows steady improvement in the accuracy of the fit. On the other hand, in figure 10 there is a clear trend visible; the number of terms is seen to decrease the scatter and the data seem to converge towards a more well-defined behaviour with diminishing magnitude. This does indeed give too much weight to the flanks and too little at the centre and this supports the contention that the limiting distribution is close to a Gaussian but given in part by a different distribution. The same trend may be tested from the RMS fit to the Gaussian. Both in the Kac model, figure 5, and to a lesser extent in the Jaynes–Cummings model, figure 13, the fidelity consistently improves when the data are extended. The K–S tests, figures 7 and 15, also behave in similar ways to each other. They converge to definite values, which is presumed to give an objective measure of the deviations between the data and the proposed distribution. These figures also show the importance of choosing a sufficiently large time t_f as n (or $\bar{n}$) is increased. Considering the numerical evidence, we see no clear indication of the emergence of an asymptotic distribution differing from the Gaussian since figures 8 and 16, show consistent improvement as n, and $\bar{n}$ increase, respectively.

In conclusion we repeat our contention that the Jaynes–Cummings time evolution shows a random Gaussian value distribution of its ensuing expectation values. To prove this numerically is a demanding endeavour, which we have tested on the Kac model where randomness is mathematically provable. We have also tried to consider honestly the possible sources of deviations from the Gaussian distribution. In spite of lingering uncertainties, we believe that the Gaussian distribution has been established beyond reasonable doubt. In any case, we feel that the results are, in their own right, interesting enough to suggest that randomness may emerge even from totally deterministic quantum dynamical evolution.

Acknowledgments

BMG would like to thank the Leverhulme Trust for financial support. SS thanks the Royal Swedish Academy of Sciences for supporting my collaboration with Sussex University, UK.

Appendix

One quantity we are interested in is the standard deviation σ given by

$$\sigma^2 = \overline{S^2(t)} - [\overline{S(t)}]^2, \tag{A.1}$$

where the time averaging is, in the numerical work, performed by periodic sampling. To determine this explicitly in the periodic sampling case we can write

$$t = k \cdot \Delta t, \tag{A.2}$$

where Δt is the sampling interval, equation (50), and k is an integer, which will run from 0 to $n_s - 1$ so that n_s is the number of time samples. Thus the final time t_f is given by

$$t_f = (n_s - 1)\Delta t. \tag{A.3}$$

For the moment we focus on $\overline{S^2(t)}$ and using equation (29) for the sum S we can explicitly write

$$\overline{S^2(t)} = \frac{1}{n_s}\sum_{k=0}^{n_s-1}\frac{2}{N^2}\sum_{m,n=0}^{\infty} c_m c_n \cos(2gt\sqrt{m})\cos(2gt\sqrt{n}). \tag{A.4}$$

Then we exchange the order of the summations and expand the cosines as exponentials so that

$$\overline{S^2(t)} = \frac{1}{2N^2 n_s}\sum_{m,n=0}^{\infty} c_m c_n \sum_{k=0}^{n_s-1}\left\{e^{i\theta^+_{m,n}k} + e^{i\theta^-_{m,n}k} + \text{c.c.}\right\} \tag{A.5}$$

where, for shorthand we define

$$\theta^{\pm}_{m,n} = \theta_m \pm \theta_n, \qquad \theta_m = 2g\Delta t\sqrt{m}. \tag{A.6}$$

Then, because this is periodic sampling we can perform the time average, i.e. the sum over k. For the pairs of terms we can use:

$$\sum_{k=0}^{n_s-1}\{e^{i\theta^{\pm}_{m,n}k} + \text{c.c.}\} = 2\frac{\cos\left[(n_s-1)\theta^{\pm}_{m,n}/2\right]\sin\left(n_s\theta^{\pm}_{m,n}/2\right)}{\sin\left(\theta^{\pm}_{m,n}/2\right)}. \tag{A.7}$$

Now we introduce a function $F(n,\theta)$ such that

$$F(n,\theta) = \frac{\cos[(n-1)\theta/2]\sin(n\theta/2)}{n\sin(\theta/2)} = \frac{1}{2n}\left[1 + \frac{\sin[(n-1/2)\theta]}{\sin(\theta/2)}\right], \tag{A.8}$$

and then

$$\overline{S^2(t)} = \frac{1}{N^2}\sum_{m,n=0}^{\infty} c_m c_n\left[F\left(n_s,\theta^+_{m,n}\right) + F\left(n_s,\theta^-_{m,n}\right)\right]. \tag{A.9}$$

A similar, but simpler argument, shows that for the first moment

$$\overline{S(t)} = \frac{1}{n_s}\sum_{k=0}^{n_s-1}\frac{\sqrt{2}}{N}\sum_{m=0}^{\infty} c_m\cos(2gt\sqrt{m}) = \frac{\sqrt{2}}{N}\sum_{m=0}^{\infty} c_m F(n_s,\theta_m). \tag{A.10}$$

In both cases the same function $F(n,\theta)$ appears. The function has some similarity to those appearing in the theory of n-slit diffraction. It has regular peaks and a maximum value of unity when the argument θ is a multiple of 2π.

In the regime of modestly large $\bar{n}$ and very large numbers of samples n_s, equations (A.9) and (A.10) provide a faster method of evaluating the standard deviation σ on a computer compared to direct averaging of the sum S. In doing so, we still assume that the scaling, or normalization, N is given by equation (44), i.e. $N^2 = \sum c_n^2$. Figure 17 shows, for an initial coherent state, both the data points of figure 12 (at the largest t_f) and a line for $\sigma - 1$ found from equations (A.9) and (A.10). We can also test the effect of increasing the density of time sampling here. Instead of equation (50), we can let $\Delta t = \epsilon/\lambda_n$, so that by reducing ϵ from unity, a higher density of time sampling is achieved. Of course, from equation (A.3), the final time t_f would shrink unless the number of samples n_s is increased correspondingly. In figure 17 we see that increasing the density of sampling by a factor of a hundred only introduces a modest change in σ. Further increases would not result in any change visible in the figure. (Note that a *decrease* in sampling density *would* produce a significant change in σ.) We also note that for $\epsilon = 1$ there is a small discrepancy between the solid line and the dots near $\bar{n} = 38$. However, this is simply because integer values of n_s are used for the data points

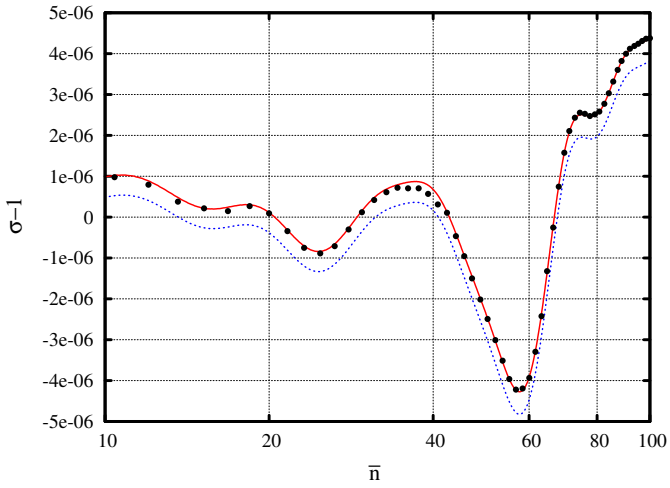

Figure 17. For the Jaynes–Cummings model we show the statistical width σ (shown as $\sigma - 1$) as a function of the mean photon number $\bar{n}$ (from 10 to 100 on a log scale). The final sample time is $t_f = 2.0 \times 10^6$ and the circles present the data from figure 12. The solid and dotted lines are derived from equations (A.9) and (A.10). The interval between sample points is given by $\Delta t = \epsilon/\lambda_n$ with $\epsilon = 1$ (solid line) and $\epsilon = 10^{-2}$ (dotted line).

marked with circles (as in figure 12), whereas, to make a smoother line, continuous values of n_s are allowed for the lines in figure 17.

For the limits of interest, $\theta \ll 1, n\theta \gg 1$ (and $gt_f \gg \sqrt{\bar{n}} \gg 1$), and an initial coherent state it is straightforward to see that in $\overline{S^2(t)}$, equation (A.9), the term $F(n_s, \theta^+_{m,n})$ contributes vanishingly for large n_s (and $\bar{n}$). Then the main contribution to $\overline{S^2(t)}$ is unity from the $F(n_s, \theta^-_{m,n})$ term when $m = n$. When $m \neq n$ it is not clear that the contributions to $\overline{S^2(t)}$ converge to zero as a function of $\bar{n}$ (as in figure 17). This is because, although the denominator of F is slowly varying in our limits, the numerator varies rapidly, i.e. changes dramatically from point to point (m, n). Nevertheless, convergence does take place as a function of n_s. The convergence to zero of equation (A.10) can also be established as a function of n_s, and thus we expect that σ converges to unity in these limits. The convergence with n_s is confirmed in figure 11 where increasing t_f, at fixed $\bar{n}$, implies increasing n_s with Δt fixed.

Figure 17 shows that σ is not especially sensitive to the sampling interval Δt, as discussed above. It is also not especially sensitive to the inevitable cut-off in the infinite sums over m (and n). At the expense of increased computation time we can increase this cut-off from, say, $2.5\bar{n}$ to $5\bar{n}$ with only a very small change in the results. However, $\sigma - 1$ is sensitive to the selected final time t_f, i.e. to the number of time samples n_s. (As already remarked, this lies behind the small difference between the circles and solid line in figure 17.) Needless to say, if we change from periodic sampling to random time sampling, whilst most of the trends seen in this paper remain very similar, the result for $\sigma - 1$ *does* change, since it loses its deterministic behaviour and increases in its range of values.

References

[1] Shore B V and Knight P L 1993 *J. Mod. Opt.* **40** 1195
[2] Ackerhalt J R, Milonni P W and Shih M-L 1985 *Phys. Rep.* **128** 205
[3] Belobrov P I, Zaslavskii G M and Tartakovskii G Kh 1976 *Sov. Phys.—JETP* **44** 945

[4] Milonni P W, Ackerhalt J R and Galbraith H W 1983 *Phys. Rev. Lett.* **50** 966
[5] Haken H 1975 *Phys. Lett.* **53A** 77
[6] Kac M 1959 *Statistical Independence in Probability, Analysis and Number Theory* (New York: Wiley)
[7] Abramowitz M and Stegun I A 1964 *Handbook of Mathematical Functions* (New York: Dover)
[8] Press W H, Flannery B P, Teukolsky S A and Vetterling W T 1986 *Numerical Recipes* (Cambridge: Cambridge University Press)
[9] Eberly J H, Narozhny N B and Sanchez-Mondragon J J 1980 *Phys. Rev. Lett.* **44** 1323